

Optimal-time Quadcopter Descent Trajectories Avoiding the Vortex Ring and Autorotation States

Amin Talaeizadeh^a, Duarte Antunes^{b,*}, Hossein Nejat Pishkenari^{a,*} and Aria Alasty^a

Abstract—It is well-known that helicopters descending fast may enter the so-called Vortex Ring State (VRS), a region in the velocity space where the blades lift differs significantly from regular regions. This may lead to instability and therefore this region is avoided, typically by increasing the horizontal speed. This paper researches this phenomenon in the context of small-scale quadcopters. The region corresponding to the VRS is identified by combining first-principles modeling and wind-tunnel experiments. Moreover, we propose that the so called Windmill-Brake State (WBS) or autorotation region should also be avoided for quadcopters, which is not necessarily the case for helicopters. A model is proposed for the velocity constraints that the quadcopter must meet to avoid these regions. Then, the problem of designing optimal time descend trajectories that avoid the VRS and WBS regions is tackled. Finally, the optimal trajectories are implemented on a quadcopter. The flight tests show that by following the designed trajectories, the quadcopter is able to descend considerably faster than purely vertical trajectories that also avoid the VRS and WBS.

Index Terms—Vortex ring state, Quadcopter, Windmill brake state, Optimal trajectory design, Vortex ring avoidance trajectory, Quadcopter fast descent.

I. INTRODUCTION

QUADCOPTERS have been introduced in recent years and are expected to have a large impact on many applications, such as agriculture monitoring, industrial inspection, entertainment industry, among others [1]. One of the interesting features of these aerial robots is that they are able to perform aggressive maneuvers due to their agility. In order to safely conduct these aggressive maneuvers, it is important to model and understand the dynamic behavior at high speeds, where non-trivial aerodynamic effects come into play.

Such aerodynamic effects have been extensively studied in the context of helicopters, where one can find several seminal papers [2]–[7]. As explained in these papers, there are three regions in the velocity space called Vortex Ring State (VRS), Windmill-Brake State (WBS) and Turbulence Wake State (TWS) in which the behavior of the helicopter and the effect of the environment is different from regular regions. The VRS and TWS regions must be avoided, but it is still possible, although undesired, to control the helicopter in the WBS region. However, these effects have received only limited

attention in the context of quadcopters, despite the fact that they can play a very important role due to their agility. Some exceptions are [8]–[16].

In [8] it is reported that for descending trajectories and for some velocity state space regions a quadcopter can become unstable. Other studies show that these instabilities are due to the VRS effects, see [9]–[11], where simple models are defined for explaining the boundary of these regions. These simple models are similar to helicopter models and are used in some works to design controllers that avoid entering the VRS [12]–[16]. In fact, these studies are similar to helicopter VRS avoiding controllers introduced in [17], [18]. However, the results of these models and control strategies have only been shown through simulation and have not been validated through real measurements. Moreover, due to differences in the blades mechanisms between helicopters and quadcopters¹, high fluctuation regions are different. Furthermore, such controllers are not time-optimal, which is often required in the context of aggressive maneuvers. (see [19]–[21] which tackle the problem of finding time-optimal trajectories without considering aerodynamic constraints.)

In this paper, we conduct static experimental tests on a wind tunnel to identify the regions where fluctuations occur. Combining this information with the VRS and TWS regions predicted by a theoretical model, we provide a simple model for the region in the velocity space to be avoided by the quadcopter. As we will discuss, we claim that the quadcopter, contrarily to helicopters, should also avoid the WBS region. According to the model for constraints and state bounds, different optimal trajectories are designed, considering planar 2D and full 3D models for the motion of the quadcopter. Due to the complexity of this nonlinear optimal control problem, we resort to the optimal control toolbox, GPOPS-II [22]. The designed trajectories to descend as fast as possible boil down to intuitive maneuvers, such as oblique and flips maneuvers in 2D, and helix type maneuvers in 3D. Finally, the optimal trajectories are implemented on a quadcopter. The flight tests show that by following the designed trajectories, the quadcopter is able to descend considerably faster than purely vertical trajectories that also avoid the VRS.

The remainder of the paper is organized as follows. In Section II, the aerodynamic effects in descent maneuvers that

^a Mechanical Engineering Department, Sharif University of Technology, Tehran, I.R.Iran

^b Control Systems Technology Group, Department of Mechanical Engineering, Eindhoven University of Technology, 5600MB Eindhoven, The Netherlands

Email addresses: amtalaiezadeh@mech.sharif.edu (A. Talaeizadeh), d.antunes@tue.nl (D. Antunes), nejat@sharif.edu (H. Nejat Pishkenari), aalasti@sharif.edu (A. Alasty).

¹The helicopters blades have a constant rotational speed and their pitch angle is variable with a swashplate mechanism for changing the direction of the blade disk thrust. In contrast, quadcopters motor speed is variable, and their blades pitch angle is usually fixed. Moreover, the hinges of the helicopter blades provide a flapping degree of freedom, whereas in contrast to the quadcopter where the blades are rigid.

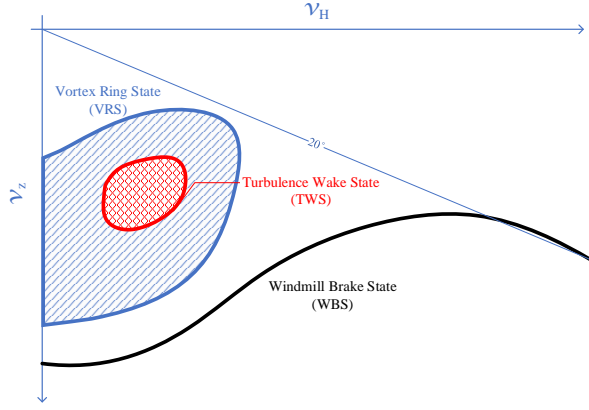


Fig. 1: The VRS, TWS and WBS regions in the velocity state space for helicopters are shown in the figure. Both vertical, v_z , and horizontal v_H speeds are normalized by the induced velocity at hover, where v_H and v_z are horizontal and vertical speeds in the blade disk frame, respectively [2].

may cause instability are described, and two major regions in the descent of quadcopters are introduced, based on a theoretical model borrowed from helicopter aerodynamic theory. In Section III, the wind tunnel test results are described and a model is suggested for the boundaries of the unstable regions in the velocity space. Section IV provides optimal minimum time trajectories in 2D and 3D spaces that are designed considering the VRS constraints, a model of the quadcopter, and GPOPS-II. Section V presents the flight test experiments by which the quadcopter follows the optimal time trajectories while avoiding the VRS. Section VI provides a brief discussion and research lines for future work.

II. MODEL OF CRITICAL REGIONS DURING DESCENT

In this section, the behavior of the quadcopter in descent maneuvers is described based on the theory available for helicopters. When a helicopter is descending, in some regions in the velocity state space, intensive vibrations and fluctuations in thrust occur. By increasing the horizontal speed of the helicopter, these effects can be reduced. Depending on the vertical and horizontal speeds, the amplitude of fluctuations in thrust can vary. The low and high amplitude fluctuations are known as VRS and TWS, respectively. In Figure 1, the VRS and TWS regions are illustrated in the velocity space normalized by the induced velocity at hover. The induced velocity corresponds to the flow at the tip of the blade from the high-pressure air at the bottom of the blade to the low-pressure air at the top of the blade. For a helicopter, the descent modes can be divided into four modes:

- *Normal Descent*: In this mode, there is no fluctuation on the thrust. This corresponds to a normal flight mode.
- *VRS*: In a descent maneuver, the first low fluctuations in the thrust are in the Vortex Ring state region. This region is described in Section II-1.
- *TWS*: In this region, because of high amplitude fluctuations on the thrust, the helicopter experiences intensive vibrations which might lead to instability. This region is

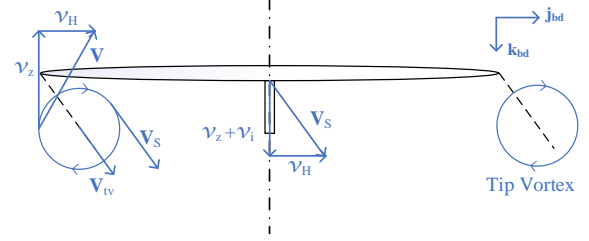


Fig. 2: Tip vortexes velocities in oblique descent, used in Onera's criterion [13]. V_S in this figure is the velocity of air stream in the blade disk.

also considered as VRS in this paper because this region is encompassed by the VRS region in the velocity state space.

- *WBS*:(or autorotation) In this region, while the helicopter still suffers high amplitude fluctuations, there is enough lift created by the airflow (contrarily to the VRS) such that the helicopter can still be controlled.² This can be achieved by switching off the motors and changing the pitch angle of the blades to simply control the angle of attack (the pilot can, e.g., change a positive angle of attack to a negative one to produce the thrust and change the thrust vector direction with the swashplate to control the orientation of the helicopter [7]). The blades lift (and rotation) will now be caused by the air moving up through the blade disk and not by the motors. This effect is equivalent to the gliding flight in fixed-wing planes. In Section II-2, the differences between helicopter and quadcopter, and the behavior of the quadcopter in this region are explained.

To determine the behavior of the quadcopter in the descent phases, firstly, we will provide a model for the VRS and TWS regions. For the WBS region, we will discuss that due to the differences between the helicopter's and quadcopter's blade disks, the WBS models for helicopters are not valid for quadcopters, and we will find the behavior of the quadcopter's blade disks by wind tunnel tests which are provided in Section III.

1) *Vortex Ring State Model in Quadcopter*: The momentum theory is not valid in the VRS and TWS regions. However, it is possible to find the boundary of these regions to identify if the quadcopter is in these regions or not. For modeling the VRS and TWS boundaries, there are many suggestions in the literature [23]–[25]. One of the closest models to the experiments is Oneras model [26]. Let $\|\mathbf{V}_{tv}\|$ be the speed of blade's tip vortex and let ϵ_{cr} be the critical velocity of the blade's tip vortexes. Then the following criterion defines the critical region [26]:

$$\|\mathbf{V}_{tv}\| \leq \epsilon_{cr}, \quad (1)$$

where the speed of blade's tip vortex can be calculated from:

$$\mathbf{V}_{tv} = v_H \mathbf{j}_{bd} + (v_i/2 + v_z) \mathbf{k}_{bd}, \quad (2)$$

²A helicopter typically enters WBS or autorotation region when it cannot use its engine because of motor's or tail-rotor's malfunctioning.

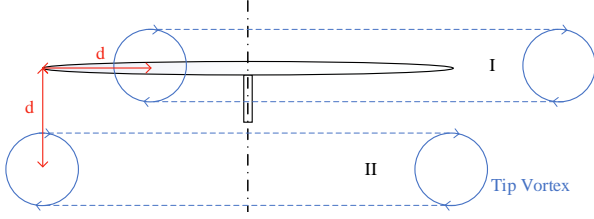


Fig. 3: Asymmetry in maneuvers with horizontal speeds pertaining to Onera's criterion for the vortex ring state model [13]. I and II are two vortex rings leaving the rotor with the same velocity, but moving in the parallel and perpendicular directions, respectively. After a time t , they will move the distance d , however Figure 3 shows that tip vortex I is still in contact with the blade disk while vortex II is not.

where v_H and v_z are the horizontal and vertical speeds in the blade disk frame, respectively, v_i is the induced velocity in the blade disk, and the unity vectors, \hat{j}_{bd} and \hat{k}_{bd} are parallel and perpendicular to the blade disk, as shown in Figure 2. Using (1), (2), the criterion can be rewritten as:

$$\|V_{tv}\| = \sqrt{V_{tv_H}^2 + V_{tv_z}^2} \leq \epsilon_{cr}. \quad (3)$$

where $V_{tv_H} = v_H$ and $V_{tv_z} = v_i/2 + v_z$. Figure 2 illustrates this setting. However, this model is not symmetric when the quadcopter has a horizontal speed, as shown in Figure 3. Let us consider I and II as two vortex rings leaving the rotor with the same velocity, but moving in the parallel and perpendicular directions, respectively. After a time t , they will move the distance d , however Figure 3 shows that tip vortex I is still in contact with the blade disk while vortex II is not.

To improve the accuracy of this model, assuming asymmetric effects, a correction coefficient, k , should be added to the criterion as introduced in the following equation:

$$\sqrt{(v_H/k)^2 + (v_i/2 + v_z)^2} \leq \epsilon_{cr}, \quad (4)$$

where k is a parameter larger than one, $k \geq 1$. Then $V_{tv_H} = v_H/k$ and $V_{tv_z} = v_i/2 + v_z$. Therefore, in order to meet (4) the following conditions are necessary:

$$\begin{cases} V_{tv_H} \leq \epsilon_H \\ V_{tv_z} \leq \epsilon_z \end{cases}, \epsilon_z \leq \epsilon_H, \quad (5)$$

where $\epsilon_H = k\epsilon_z$ and $\epsilon_z = \epsilon_{cr}$. ϵ_z and ϵ_H are critical blade's tip vortex velocity in pure vertical and horizontal maneuvers, respectively. To calculate the induced velocity, the following equation can be used [4]:

$$v_i \sqrt{v_H^2 + (v_i + v_z)^2} = v_h^2, \quad (6)$$

where v_h is given constant coinciding with the induced velocity in the blade disk at hover and can be calculated as:

$$v_h = \sqrt{T_{Hover}/2\rho A}, \quad (7)$$

where T_{Hover} is the thrust of the motor at hover, ρ is the air density, and A is the blade disk area. Usually, T_{Hover}/A is denoted by the disk load. Let

$$\epsilon = \sqrt{(v_H/k)^2 + (v_i/2 + v_z)^2}. \quad (8)$$

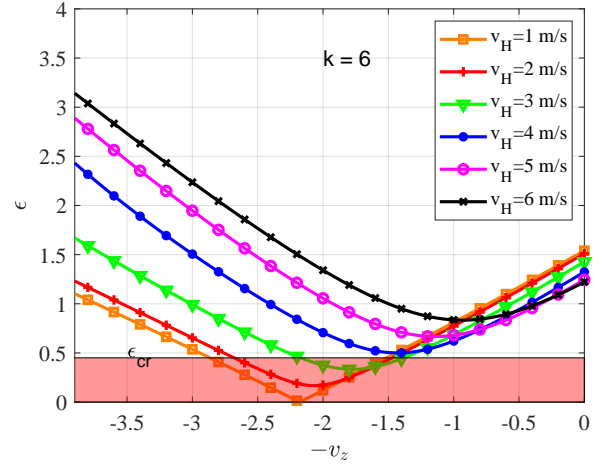


Fig. 4: Variation of ϵ based on different values of v_H and v_z . The effect of the horizontal speed in the blade disk frame is obvious, more horizontal speed, more ϵ value. In this figure, $T_{Hover} = 0.5 \text{ kg}$, $\rho = 1.2 \text{ kg/m}^3$, and the blade disk diameter is 0.2 m .

If we fix v_H , we can compute v_i as a function of v_z from (6) and plot ϵ , as a function of v_z . This plot is shown in Figure 4 for different values of v_H . This figure illustrates that by increasing the horizontal speed in the blade disk frame v_H , the ϵ value will increase and therefore it is possible to increase the vertical (descent) speed v_z without entering the VRS and TWS regions. Such regions are defined by $\epsilon \leq \epsilon_{cr}$, and are also depicted in Figure 4.

Figure 5 shows the numerical solution of criterion (4) with $k = 6$ and $\epsilon_{cr} = 0.4$ for the VRS (which illustrates with orange stars) and $\epsilon_{cr} = 0.2$ for the TWS (which illustrates with red circles). The induced velocity is calculated from (6). Figure 5 illustrates the VRS and TWS based on Onera's criterion. Note that following Onera's criterion one cannot identify the WBS which is a limitation of this theoretical model. Such a region will be identified experimentally in the next section. Since the TWS is encompassed by the VRS, we will simply consider the union of these regions as a prohibited region and denoted this region simply by the VRS region.

2) Windmill Brake State in quadcopters: As explained before, the control of a helicopter in this region is achieved by changing the pitch. This is possible due to the pitch angle degree of freedom in the helicopters blade mechanism. However, for quadcopters, there is no degree of freedom in pitch angles, and there is not a swashplate mechanism to handle the thrust vector in the absence of the motor. Since if we turn off the motors of the quadcopter, we will lose the controllability of the quadcopter, the autorotation effect acts as a brake in the blade disk. In the autorotation mode, by the action of upward air, the blades tend to rotate in the opposite direction, the motor performs torque to turn the blades and this may cause fluctuations on the blade disk. Hence, WBS regions should be considered as a forbidden area for quadcopters like the VRS and TWS regions.

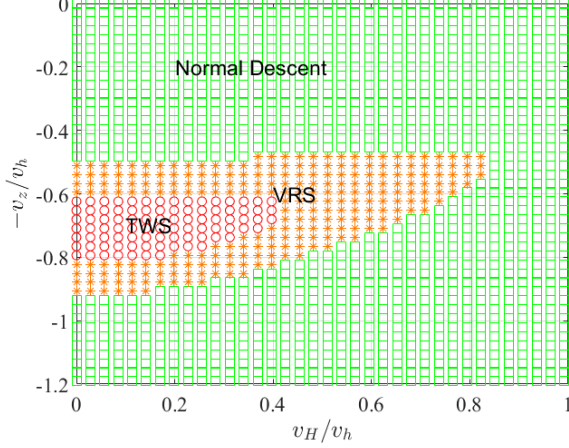


Fig. 5: Numerical solution of the Oneras criterion. The VRS and TWS are illustrated by orange stars and red circles, respectively. The region identified with green squares corresponds to normal descent in Onera's criterion, however this region may include WBS in reality. In this figure, $T_{Hover} = 0.5 \text{ kg}$, $\rho = 1.2 \text{ kg/m}^3$, and the blade disk diameter is 0.2 m .

III. IDENTIFICATION OF THE DESCEND REGIMES IN THE QUADCOPTERS

To identify the behavior of the brushless motors with fixed pitch angle blades, in different descent velocities and angles, an experimental setup has been designed, see Figure 6. This experimental setup can measure the force of motor-blades, rpm, current, voltage. The angle of the setup can be modified so that it emulates the oblique descent in the wind tunnel, see Figure 7. For these experiments, the wind tunnel of the Eindhoven University of Technology (TU/e) is used. In this wind tunnel, we measured the amount of thrust and its fluctuation, the motor rpm, and the motor Pulse Width Modulation (PWM) and voltage input in different wind velocities and different setup angles (to simulate the different angles of descent). These tests were performed with different blades and motors. However, the results, illustrated in Figure 8 are for T-Motor Air 2213 brushless motor and T9545 Propeller. The results are normalized by the induced velocity at hover. Regions with high fluctuations ($\Delta T/T \geq 10\%$ for thrust fluctuations) are defined as prohibited regions.

As predicted, based on the theoretical analysis, high fluctuations occur in the VRS region computed from the Oneras criterion. Interestingly, fluctuations also occur in the blue regions shown in Figure 8, which is identified as the WBS (which as mentioned before, is not predicted from Oneras model). As also depicted in Figure 8, and also in Figure 9, we can define a simplified region where high fluctuations do not occur. This is summarized in the next definition.

Definition 1. *Simplified VRS Velocity Constraint*

$$\begin{aligned} |v_H| \tan 20^\circ &\geq v_z, \\ \forall v_z \leq 0, v_H &\in \mathbb{R}, \end{aligned} \quad (9)$$

where v_H and v_z are in the body fixed frame.

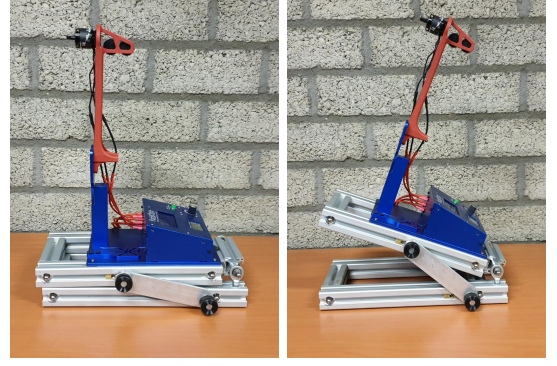


Fig. 6: Motor-blade tester to measure thrust, rpm, voltage and PWM adapted for simulating various oblique descent angles in wind tunnel. Setup angle is measured by a digital inclinometer.

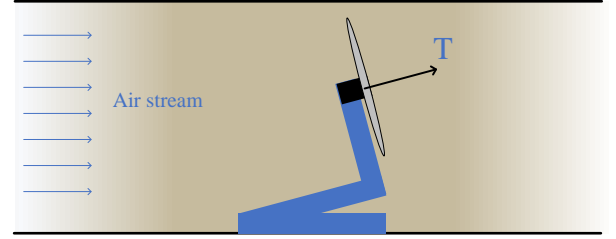


Fig. 7: Emulation of descent in wind tunnel with variable angle mechanism for thrust tester setup.

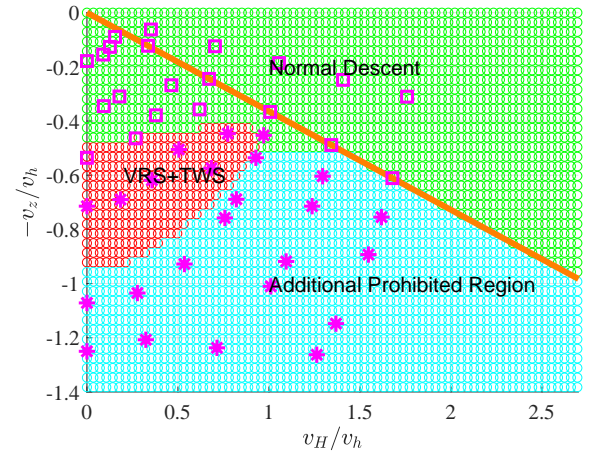


Fig. 8: Wind tunnel experiment results where stars and squares define the high fluctuation and low fluctuation points, respectively. The VRS region, using the Onera's criterion is illustrated with red color. The blue color region is also prohibited due to the high fluctuations, and it concluded in this research that these fluctuations are the WBS effect. Normal regions are depicted by green color. To simplify this constraint, the top region of the orange line is considered as the allowable region

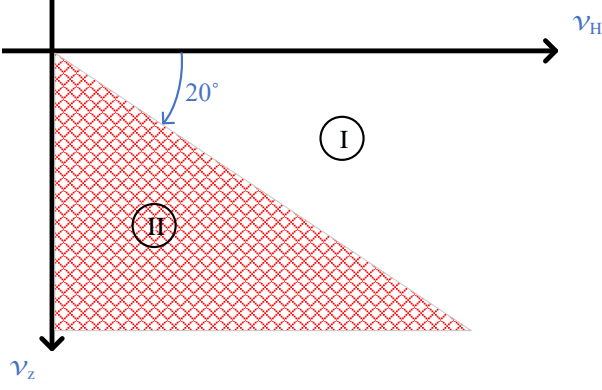


Fig. 9: The simplified constraint used for optimal trajectory design. Regions I and II are allowed and prohibited regions, respectively.

Remark 1. The motion planner should design a trajectory to avoid these regions. Note that to take into account these constraints it is necessary to compute the relative wind velocities in the blade disk frame, not in the inertial frame, as it will be discussed in the next section.

Remark 2. The dimensions of the velocity constraints are normalized by the induced velocity at hover. Therefore, this model can be used for every kind of quadcopters' blade disks with different disk loads and diameters that have fixed-pitch blades.

IV. DESIGN OF OPTIMAL TRAJECTORIES

This section tackles the problem of designing optimal trajectories for a quadcopter to descend as fast as possible, considering the VRS and WBS constraints. Section IV-A provides the equations of motion of a quadcopter. In Section IV-B and Section IV-C, the motion of the quadcopter is considered in 2D and 3D space, respectively, and descend trajectories with minimum time are designed.

A. Quadcopter Equations of Motion

If we consider the North-East-Down (NED) as the inertial frame, and a body fixed frame, denoted by b with its origin coinciding with the center, z axis aligned with the gravitational vector when the quadcopter is at hover and x and y axis as shown in Figure 10, the total external force \mathbf{F}^I expressed in the inertial frame acting on the quadcopter can be expressed as follows (see [27]):

$$\sum \mathbf{F}^I = \mathbf{R}_b^I \begin{Bmatrix} 0 \\ 0 \\ \sum_{i=1}^4 (-T_i) \end{Bmatrix} + \begin{Bmatrix} 0 \\ 0 \\ mg \end{Bmatrix} + \mathbf{F}_{\text{ext}}, \quad (10)$$

where \mathbf{F}_{ext} is disturbance force vector, \mathbf{R}_b^I is the rotation matrix from the body to the inertial frame and T_i denotes the thrust generated by the i^{th} motor.

By the Euler-Newton formalism, the summation of torques that are applied to the quadcopter is equal to the time rate of

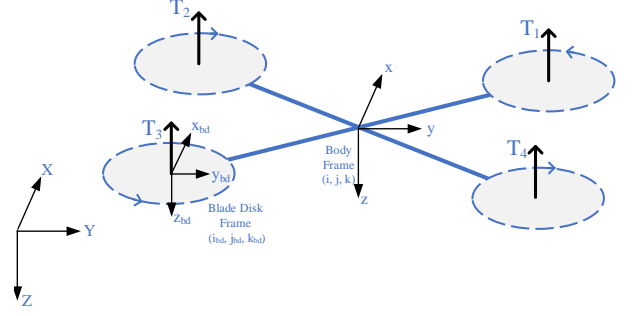


Fig. 10: Quadcopter, its motors' thrusts, the inertial, body and blade disk NED frames are illustrated.

change of the angular momentum.

$$\sum \mathbf{M} = d\mathbf{H}/dt = \dot{\mathbf{H}} + \boldsymbol{\omega} \times \mathbf{H}. \quad (11)$$

The torques that are applied to the robot from motors depend on the configuration of the quadcopter. For an X shaped quadcopter, the torques are given by:

$$\mathbf{M} = \begin{Bmatrix} M_x \\ M_y \\ M_z \end{Bmatrix} = \begin{Bmatrix} b(-T_1 + T_2 + T_3 - T_4) \\ b(T_1 + T_2 - T_3 - T_4) \\ (-M_1 + M_2 - M_3 + M_4) \end{Bmatrix} + \mathbf{M}_{\text{ext}}, \quad (12)$$

where T_i is the output thrust of the i^{th} motor, b is the distance between motors and center of gravity, M_i is the output torque of i^{th} motor and \mathbf{M}_{ext} is the external torque vector. In (11), \mathbf{H} is the angular momentum of the robot that can be calculated as:

$$\mathbf{H} = \mathbf{I}\boldsymbol{\omega}, \quad (13)$$

where \mathbf{I} is the body's inertia tensor of the quadcopter, and $\boldsymbol{\omega}$ is the angular velocity of the quadcopter's body.

$$\boldsymbol{\omega} = \begin{Bmatrix} \omega_x \\ \omega_y \\ \omega_z \end{Bmatrix} = \begin{Bmatrix} p \\ q \\ r \end{Bmatrix}. \quad (14)$$

Therefore, equation (11) can be rewritten as:

$$\sum \mathbf{M} = \mathbf{I}\dot{\boldsymbol{\omega}} + \mathbf{S}(\boldsymbol{\omega})\mathbf{I}\boldsymbol{\omega}, \quad (15)$$

where

$$\mathbf{S}(\boldsymbol{\omega}) = \begin{bmatrix} 0 & -r & q \\ r & 0 & -p \\ -q & p & 0 \end{bmatrix}. \quad (16)$$

Finally, the equations of motion are given by:

$$\begin{aligned} \dot{\mathbf{P}} &= \mathbf{V}, \\ \dot{\mathbf{V}} &= \sum \mathbf{F}^I/m, \\ \dot{\mathbf{R}}_b^I &= \mathbf{R}_b^I \mathbf{S}(\boldsymbol{\omega}), \\ \mathbf{I}\dot{\boldsymbol{\omega}} &= \sum \mathbf{M} - \mathbf{S}(\boldsymbol{\omega})\mathbf{I}\boldsymbol{\omega}, \end{aligned} \quad (17)$$

where \mathbf{P} and \mathbf{V} are the position and the velocity of the quadcopter's center of mass in the inertial frame, respectively, and m is the quadcopter's mass.

Alternatively to the equation $\dot{\mathbf{R}}_b^I = \mathbf{R}_b^I \mathbf{S}(\boldsymbol{\omega})$, we can write:

$$\dot{q} = \mathbf{G}(q)\boldsymbol{\omega}, \quad (18)$$

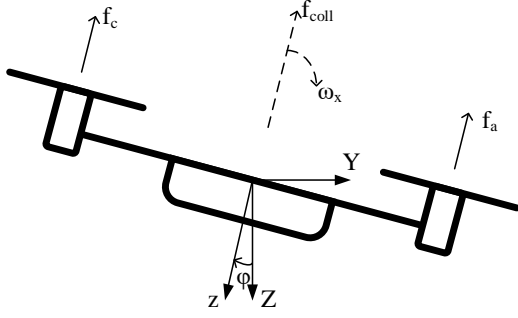


Fig. 11: Quadcopter in 2D analysis, including two motors. The inertial and body frames are illustrated.

where $q = [q_0, q_1, q_2, q_3]$ are the quaternions and $G(q)$ is a matrix of quaternions [28].

B. 2D Optimal Trajectories

Consider the quadcopter is in the Y-Z plane, as shown in Figure 11, its motion is planar and there are only three degrees of freedom. Let us combine two pairs of motors on each side, so that we can assume a single thrust force is applied on each side. Although this leads to a simple planar model, it is still an underactuated system, such as the full 3D quadcopter model. The equations of motion for this simplified can be derived from the full model (17) and are given by:

$$\begin{aligned}\ddot{Z} &= -f_{coll} \cos \phi + g, \\ \ddot{Y} &= f_{coll} \sin \phi, \\ I_{xx} \ddot{\phi} &= ml(f_a - f_c),\end{aligned}\quad (19)$$

where f_{coll} is the collective acceleration from the motors' thrusts:

$$f_{coll} = f_a + f_c, \quad (20)$$

where f_a and f_c are the thrusts of each motor, divided by the mass. If we assume the angular velocity as a control input, the kinematic equation can be assumed to be simply given by:

$$\dot{\phi} = \omega_x. \quad (21)$$

The system states, S , and inputs, U , are:

$$\begin{aligned}S &= (Y, V_Y, Z, V_Z, \phi), \\ U &= (f_{coll}, \omega_x).\end{aligned}\quad (22)$$

The state space equation is:

$$\begin{aligned}\begin{bmatrix} \dot{Y} \\ \dot{V}_Y \\ \dot{Z} \\ \dot{V}_Z \\ \dot{\phi} \end{bmatrix} &= \begin{bmatrix} 0 & 1 & 0 & 0 & 0 \\ 0 & 0 & 0 & 0 & 0 \\ 0 & 0 & 0 & 1 & 0 \\ 0 & 0 & 0 & 0 & 0 \\ 0 & 0 & 0 & 0 & 0 \end{bmatrix} \begin{bmatrix} Y \\ V_Y \\ Z \\ V_Z \\ \phi \end{bmatrix} + \\ &\quad \begin{bmatrix} 0 \\ \sin \phi \\ 0 \\ -\cos \phi \\ 0 \end{bmatrix} \begin{bmatrix} f_{coll} \\ \omega_x \end{bmatrix} + \begin{bmatrix} 0 \\ 0 \\ 0 \\ g \\ 0 \end{bmatrix}\end{aligned}\quad (23)$$

Our goal is to design a control law for the quadcopter to move from the initial state at height h_1 to the final state at height h_2 both at hover.

The cost function for the optimal trajectory design, J , is for the minimum time problem:

$$J = \min \int_0^{t_f} g(S, U) dt = \min \int_0^{t_f} 1 dt. \quad (24)$$

Taking into account the relation between velocities in the body fixed frame (v_H, v_z) and the inertial frame (V_Y, V_Z):

$$\begin{pmatrix} v_H \\ v_z \end{pmatrix} = \begin{bmatrix} \cos \phi & -\sin \phi \\ \sin \phi & \cos \phi \end{bmatrix} \begin{pmatrix} V_Y \\ V_Z \end{pmatrix}, \quad (25)$$

we can consider the simplified velocity constraint (9), $C(V_Y, V_Z, \phi) \geq 0$, where:

$$C(V_Y, V_Z, \phi) = V_Z(1 - B \tan \phi) - V_Y(B + \tan \phi), \quad (26)$$

and $B = \tan(20^\circ)$. This constraint is obtained by finding the air relative velocity in the body fixed frame and using the Definition 1. To take into account this constraint we modify the Hamiltonian to:

$$H(S, U, \lambda) = g(S, U) + \lambda^T f(S, U) + \lambda_C C(V_Y, V_Z, \phi), \quad (27)$$

where λ denotes the co-state variables:

$$\lambda = [\lambda_Y \quad \lambda_{V_Y} \quad \lambda_Z \quad \lambda_{V_Z} \quad \lambda_\phi]^T. \quad (28)$$

Using cost function, dynamic and path equations, the Hamiltonian can be written as:

$$\begin{aligned}H(S, U, \lambda) &= 1 + \lambda_Y V_Y + \lambda_{V_Y} (f_{coll} \sin \phi) + \lambda_Z V_Z \\ &\quad + \lambda_{V_Z} (-f_{coll} \cos \phi + g) + \lambda_\phi \omega_x + \\ &\quad \lambda_C (V_Z(1 - B \tan \phi) - V_Y(B + \tan \phi)).\end{aligned}\quad (29)$$

Using the Maximum Principle for problems with mixed inequality constraints conditions [29] and Hamiltonian in (29), we obtain:

$$\begin{aligned}\dot{\lambda}(t) &= -\frac{dH}{dS}(S^*(t), U^*(t), \lambda(t))^T, \\ \dot{\lambda}_Y &= 0 \rightarrow \lambda_Y = c_1, \\ \dot{\lambda}_{V_Y} &= -\lambda_Y + \lambda_C (B + \tan \phi), \\ \dot{\lambda}_Z &= 0 \rightarrow \lambda_Z = c_3, \\ \dot{\lambda}_{V_Z} &= -\lambda_Z - \lambda_C (1 - B \tan \phi), \\ \dot{\lambda}_\phi &= f_{coll} (-\lambda_{V_Y} \cos \phi - \lambda_{V_Z} \sin \phi) \\ &\quad - \lambda_C / (\cos \phi)^2 (V_Z B - V_Y),\end{aligned}\quad (30)$$

where $\lambda_C \geq 0$ and $\lambda_C C(V_Y, V_Z, \phi) = 0$ are complementary slackness conditions, and c_1 and c_3 are constants.

This problem is very complex and it is hard to solve this nonlinear optimal control problem analytically, so we use a numerical method to solve it. Namely, we used GPOPS-II, a Matlab plugin, to solve this optimization problem. GPOPS-II implements a new class of variable-order Gaussian quadrature methods where a continuous-time optimal control problem is approximated as a sparse Nonlinear Programming (NLP) problem [22].

Besides the constraints corresponding to the dynamics (23), the constraint that should be satisfied during the whole path is (26).

TABLE I: Initial and final values as well as admissible intervals of the system variables

Variable	Initial Cond.	Final Cond.	Admissible Intervals
Y	0	0	$[-15, 15]$
V_Y	0	0	$[-10, 10]$
Z	0	5	$[-15, 15]$
V_Z	0	0	$[-10, 10]$
ϕ	0	0	$[-\pi/3, \pi/3]$
f_{coll}	g	g	$[-20, 20]$
ω	0	0	$[-1, 1]$

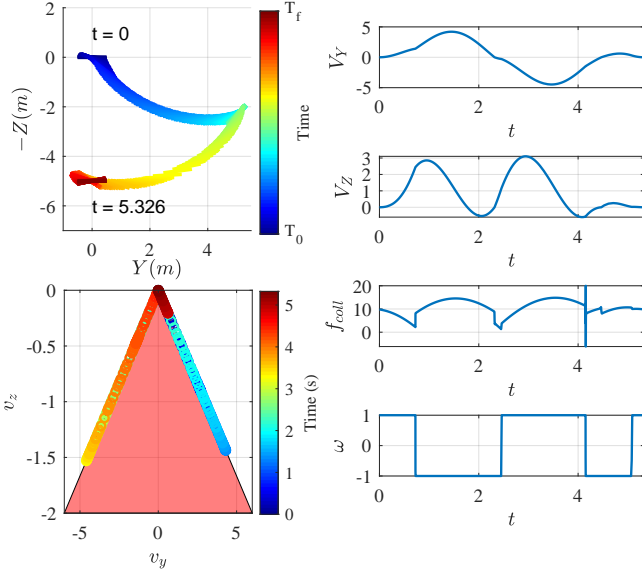


Fig. 12: Optimal 2D trajectory design for equal initial and final Y position is shown for the whole trajectory with blue to red colors. The velocity constraint, considering the velocities in the blade disk is satisfied.

Initial, final and admissible intervals of the system variables are defined in Table I. According to these initial and final values and bounds, the minimum time trajectory can be designed. With this trajectory, the quadcopter can descend 5 meters in 5.33 seconds. The simulation results and designed optimal trajectory are shown in Figure 12. This figure illustrates that even if the final horizontal displacement is not desired, the quadcopter should move in the horizontal direction meanwhile and come back to its initial Y , in order to satisfy the velocity constraint. It shows that the pure descent (without any horizontal displacement during the trajectory) is not the fastest trajectory to descend.

Moreover, if we assume that the final Y -position is free, but bounded between $[-2, 2]$, $[-5, 5]$ or $[-10, 10]$ meters, depending on the bounds, the designed trajectories are either Zig-Zag or pure oblique trajectories as illustrated in Figure 13. For the mentioned bounds, the time of the optimal trajectory is 6.80, 4.60 and 3.39 seconds, respectively. It is obvious that the pure oblique trajectory is faster than the Zig-Zag trajectories, but the latter requires a much smaller space in the 2D space. Also, by decreasing the admissible interval in the horizontal direction,

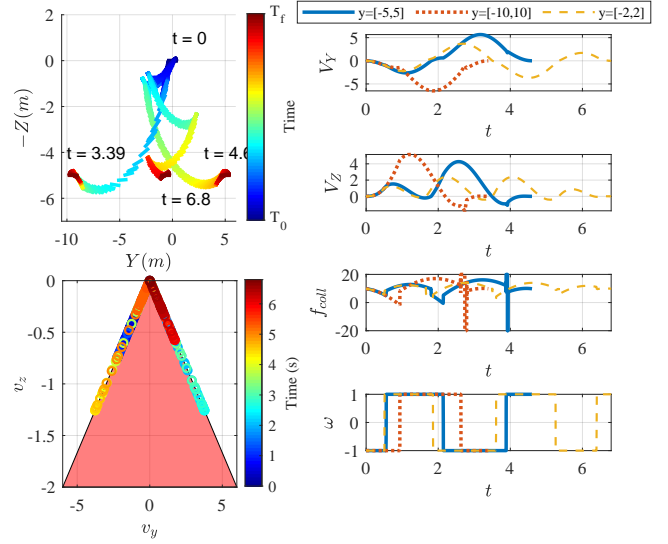


Fig. 13: Optimal 2D trajectories design for free (final Y is not fixed but it is bounded) and bounded horizontal displacement, that let the system have oblique and Zig-Zag trajectories, respectively. Moreover, the ϕ interval is $[-\pi/3, \pi/3]$. It is obvious that if the pure oblique descent is allowed, then the trajectory will be faster than Zig-Zag maneuver. Moreover, by increasing the horizontal displacement limitation, the trajectory duration will be increased.

the optimal trajectory time will increase.

Also, if we assume that the ϕ angle is free, it is permissible that the system has flip maneuvers in its trajectory. With this assumption, the optimal time of the optimal trajectory is 2.27 seconds. Figure 14 illustrates that the trajectory with flips when the system has freedom in the ϕ angle; however it should come back to its initial Y position because of predefined final conditions. Due to the upside down maneuver, the quadcopter can descend with an acceleration higher than the gravity. Moreover, because of this rotation, the descent velocity will be positive in the body fixed frame where there is no velocity constraint in positive body fixed frame z velocity region and the quadcopter can descend freely with high velocity.

Finally, if we assume that the Y displacement is free as well as the ϕ angle, the trajectory would be a combination of the oblique and flip maneuvers, illustrated in Figure 15. This trajectory takes 2.07 seconds for descending 5 meters. It shows that the fastest trajectory is a trajectory, including flips and oblique maneuvers. A comparison between methods depending on admissible intervals and allowed maneuvers, is provided in Table II.

Based on a brief review of different optimal trajectories, provided in Table II, it is evident that the fastest trajectory is a trajectory including flips and oblique maneuvers, when there are no limitations in the horizontal direction. Moreover, the lowest-speed trajectory is the Zig-Zag trajectory when there are strict limitations on the Y displacement. However, if

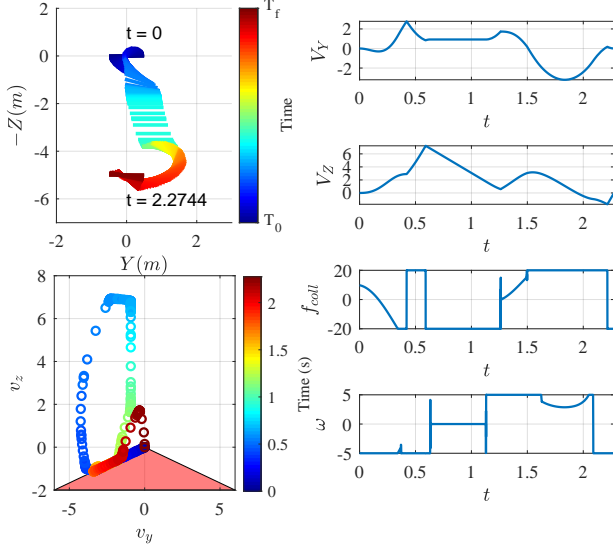


Fig. 14: Optimal 2D trajectory design for equal initial and final Y , no limitation is considered for ϕ allowing for flip maneuvers. It shows that although the final Y is fixed and equal to initial Y , the trajectory with flips is faster than ones with simple oblique maneuvers as illustrated in Figure 13. That is because of the maximum acceleration in the vertical direction is gravitational acceleration, however using flips, the quadcopter can use its thrusts to increase the acceleration in the downward direction.

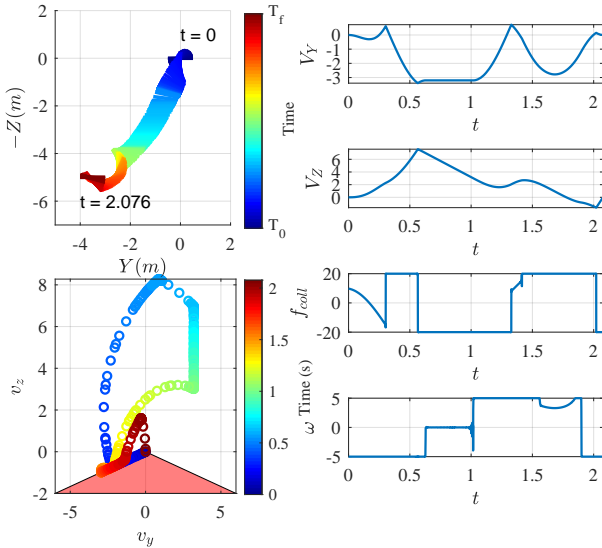


Fig. 15: Optimal 2D trajectory design with no limitation on final Y , horizontal displacement, and ϕ angle interval, allowing for oblique and flips maneuvers, simultaneously. We can see that using oblique maneuver in the combination of flip maneuvers can decrease the final trajectory time. This trajectory is the fastest trajectory that can be designed using the mentioned assumptions, limitations and constraints.

TABLE II: Optimal trajectories with different maneuvers and admissible intervals, to descend 5 meters in the Z direction. Initial and final ϕ angles are zero, as well as initial Y condition.

Y Intervals	ϕ Intervals	Final Y	Ob.	Z.Z.	Fl.	Traj. Dur.
$[-15, 15]$	$[-\pi/3, \pi/3]$	fixed(0)	\times	\checkmark	\times	5.33 s
$[-2, 2]$	$[-\pi/3, \pi/3]$	bounded	\times	\checkmark	\times	6.80 s
$[-5, 5]$	$[-\pi/3, \pi/3]$	bounded	\times	\checkmark	\times	4.60 s
$[-10, 10]$	$[-\pi/3, \pi/3]$	free	\checkmark	\times	\times	3.39 s
$[-15, 15]$	free	fixed(0)	\times	\times	\checkmark	2.27 s
$[-15, 15]$	free	free	\checkmark	\times	\checkmark	2.08 s

the flip maneuver is not allowed in the trajectory, the simple oblique trajectory will be the fastest solution for a fast descent, considering the velocity constraint.

C. 3D Optimal Trajectories

As we have shown in the 2D analysis, the fastest trajectory is the trajectory where ϕ and Y are free. However, if aggressive maneuvers are not desired, we should limit the allowed rotation angle of the quadcopter. In the 2D analysis, between the limited ϕ trajectories, Y free trajectories are the fastest. However, in real flights, the quadcopter needs to descend fast, mostly we do not have enough space for such large movement in the Y direction, in confined environments, these trajectories are not possible. As we shall see shortly, the trajectories we will obtain in this 3D analysis are helix type trajectories. Note that for helix type trajectories, a centrifugal force is also present.

Due to the centrifugal force in helix type trajectory, the quadcopter should have a pitch angle around the y axis of body frame in addition to a roll rotation around x . The thrust vector in the inertial frame is:

$$\mathbf{T}^I = \mathbf{R}_b^I \begin{bmatrix} 0 \\ 0 \\ -T \end{bmatrix}. \quad (31)$$

If the yaw angle is such that the velocity vector belongs to the xz plane in body fixed coordinates, then the component of thrust for the centrifugal force can be calculated from:

$$|\mathbf{T}_{\text{cent}}| = \left(\sum \mathbf{F}^I \right) \cdot \mathbf{e}_n \quad (32)$$

where \mathbf{T}_{cent} is the component of the thrust vector in the centrifugal direction, and \mathbf{e}_n is the unity vector perpendicular to the trajectory curve, toward to the curvature center. The magnitude of centrifugal force is:

$$\|\mathbf{T}_{\text{cent}}\| = mV^2/r. \quad (33)$$

where r is the radius of the trajectory curve each time. For finding the quadcopter velocity in the body frame, by assuming that the heading of the robot is in the forward direction of motion, we can use the rotational matrices. The wind velocity with respect to the quadcopter body in the inertial frame is:

$$\mathbf{V}_{\text{Wrel}}^I = \mathbf{W} - \mathbf{V}, \quad (34)$$

where \mathbf{W} is the wind speed, and \mathbf{V} is the quadcopter's velocity. To find the wind velocity in the body frame, we can use:

$$\mathbf{V}_{\text{Wrel}}^b = \mathbf{R}_I^b \mathbf{V}_{\text{Wrel}}^I, \quad (35)$$

where \mathbf{R}_I^b is the rotation matrix from the inertial to the body frame.

Using the velocity constraint defined in (9), the constraint in the 3D analysis will be:

$$|\mathbf{V}_{WH}^b| \tan 20^\circ \geq V_{Wz}^b, \quad (36)$$

where:

$$\begin{pmatrix} V_{Wx}^b \\ V_{Wy}^b \\ V_{Wz}^b \end{pmatrix} = \mathbf{R}_I^b \begin{pmatrix} V_X \\ V_Y \\ V_Z \end{pmatrix}, \quad (37)$$

and:

$$V_{WH}^b = \sqrt{(V_{Wx}^b)^2 + (V_{Wy}^b)^2}. \quad (38)$$

To solve the optimal-time problem for finding the fastest descent trajectory, the cost function in (24) is used. The states and control inputs in the 3D analysis are defined as:

$$\begin{aligned} S &= (X, V_X, Y, V_Y, Z, V_Z, q, \dot{q}), \\ U &= (T_1, T_2, T_3, T_4). \end{aligned} \quad (39)$$

Note that quaternions were used to avoid singularities. Moreover, if we use the equations of motion in 3D space provided in Section IV-A, considering the VRS velocity constraint in (9), we will find more complex Hamiltonian conditions that are very difficult to solve analytically. Then, numerical methods are used as for the 2D analysis. Using the GPOPS-II as the numerical solver to find the optimal trajectory, in 3D motion, the helix type trajectory can be generated for minimum time trajectory, illustrated in Figure 16. For this design, 5 meters descent and coming back to its initial X and Y positions are desired. As we have seen in the 2D analysis, for non-flip trajectories, the oblique trajectory is the fastest way to descend. Hence, in 3D analysis, the helix type trajectory is the equivalent of oblique in 2D, with consideration of Y -displacement limitation. Then, in real 3D flights, an appropriate non-aggressive (without flips) maneuver for fast descent is a helix type. This trajectory helps motion planners to design a faster descent in their mission, and it is considered for flight experiments.

V. EXPERIMENTS

For real flight tests, the Parrot Mambo drone shown in Figure 17 was utilized. This quadcopter has the following sensors: IMU, barometer, ultrasound, and a downward camera using optical flow algorithm for positioning. The controller and designed trajectories are uploaded on the Mambo from Matlab/Simulink via Bluetooth.

The mass of the Mambo quadcopter is 63 gr, and each blade disk diameter is 6.5 cm. Using the equation (7), the induced velocity at hover is 1.54 m/s.

To show the fluctuations and instability in the VRS and WBS regions in the real flight, a sinusoidal desired trajectory in the Z direction with increasing frequency is designed, which is given by:

$$Z_{des} = A \sin(\omega t) + Z_0, \quad (40)$$

where $\omega = \omega_0 t$.

By using reference, the vertical speed would grow slowly, and we can see the effects of entering the prohibited regions, in a limited flight space.

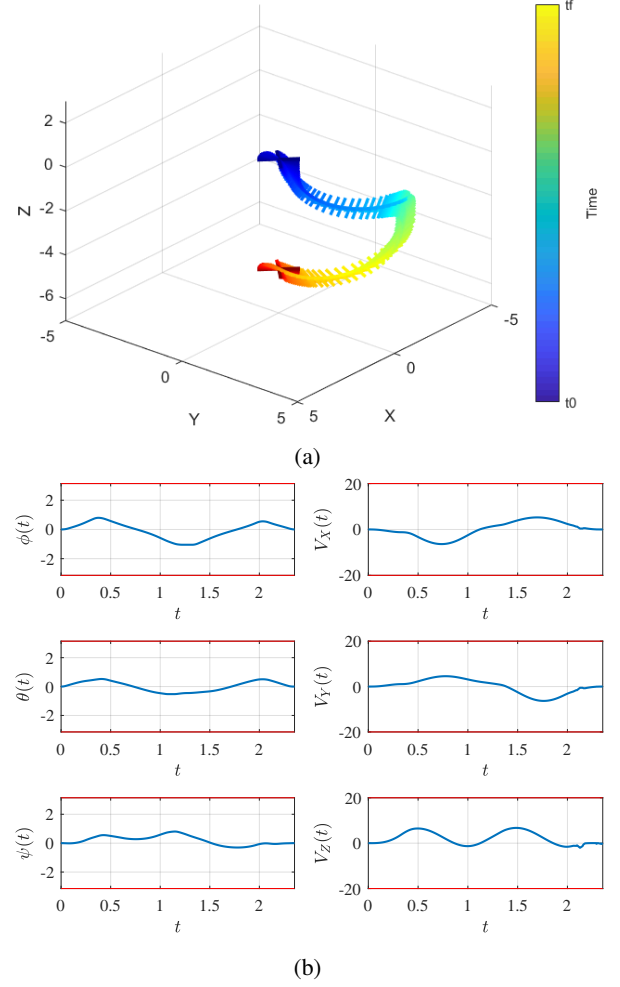


Fig. 16: Optimal 3D trajectory design for fast descent using GPOPS-II, a) Position and 3D Trajectory of generated trajectory, b) Orientation and velocity of the quadcopter in the generated trajectory.

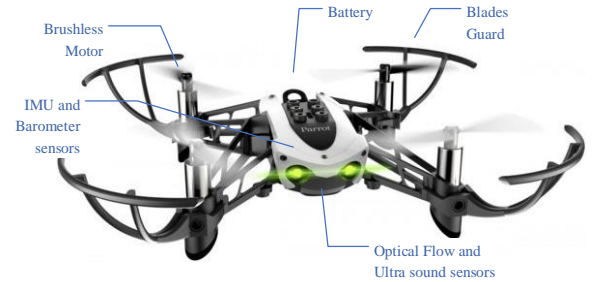
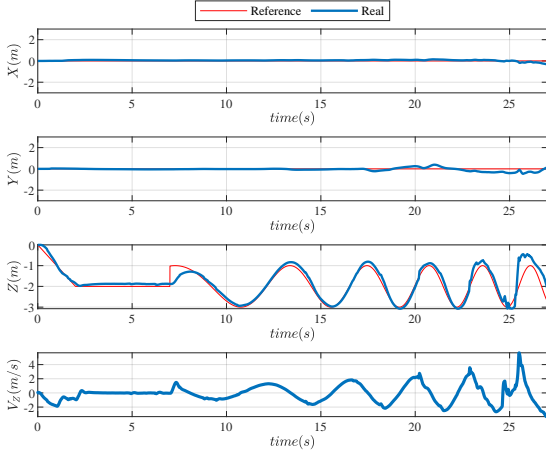
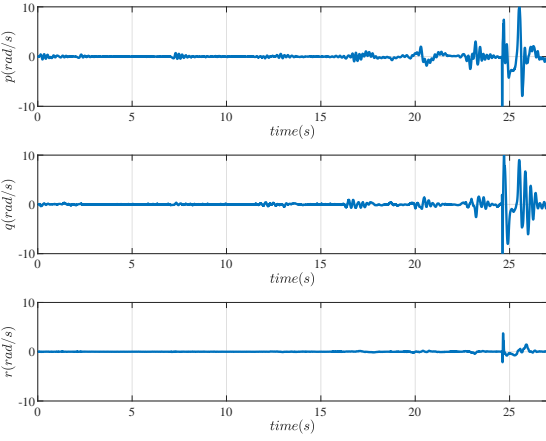


Fig. 17: Parrot Minidrone Mambo used for the flight tests



(a) Position and vertical velocity of the flying Quadcopter



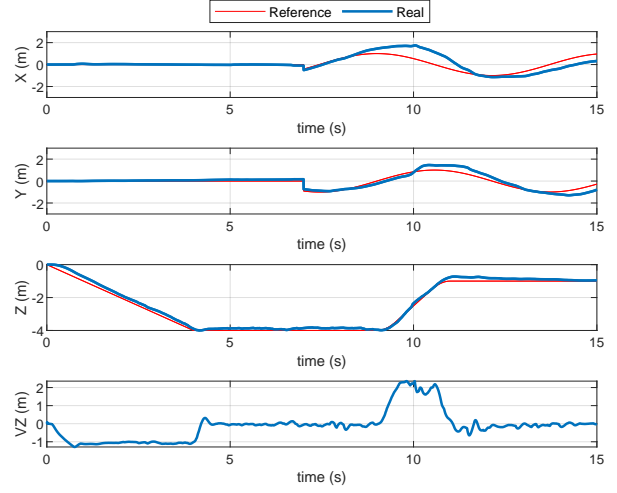
(b) Angular velocity of the quadcopter

Fig. 18: Flight tests with variable frequency sinusoidal trajectory in the Z direction that provides increasing descent velocity. This test shows that by entering into the VRS or TWS regions, the quadcopter experiences fluctuation and by increasing descent velocity, without any horizontal maneuver, the fluctuations are higher till the system becomes completely unstable, at time 24 s.

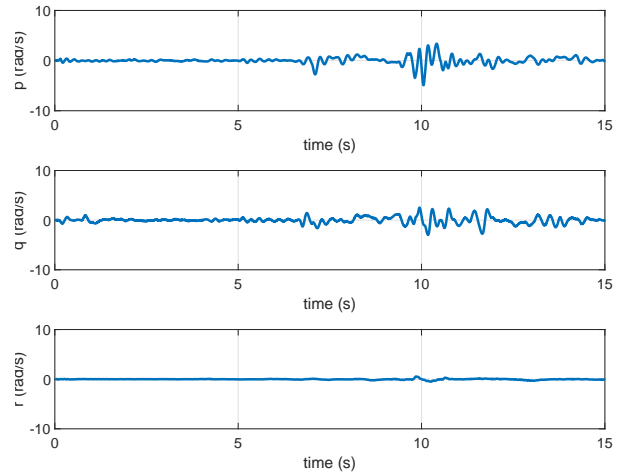
As we can see in Figure 18, by entering into the VRS region (that is 0.6 m/s velocity in the Z direction), there will be low fluctuations in the quadcopter. Entering deeper into the VRS and WBS regions, more fluctuations are experienced by the quadcopter, till the quadcopter becomes completely unstable, and crashes at 24 seconds. The data in the plots after this moment (24 seconds) pertain to the crashing effects with the ground.

This experiment shows that the VRS and WBS regions are present in the quadcopter and for the trajectory design for these rotary-wing drones, it is vital to assume the velocity constraint.

To descend as fast as possible, avoiding the VRS and WBS regions, and assuming non-aggressive maneuvers, a helix type trajectory is suggested from the analysis provided in the previous section. We can see that in Figure 19 even by having descent velocity higher than 0.6 m/s for more than 2 seconds, it can descend fast. Therefore by following a helix type trajectory



(a) Position and vertical velocity of the flying quadcopter



(b) Angular velocity of the quadcopter

Fig. 19: Drone with a helix type trajectory for achieving the high speeds in descent. It is illustrated that by following the helix type trajectory, the quadcopter can achieve high descent speeds considering the VRS and WBS constraints on air stream velocities in the blade disk frame.

and thereby adding horizontal speed in the blade disk frame the quadcopter avoids the VRS and WBS regions and does not become unstable.

In the regular descent, the quadcopter can descend 5 meters with a pure descent in 8.3 seconds. However, using VRS avoiding trajectory, the quadcopter can descend 5 meters in 2.5 seconds which is much less than the pure descent.

VI. CONCLUSIONS

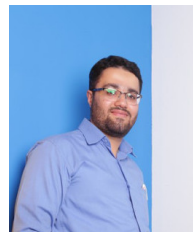
In this paper, the existence of the VRS and WBS in the context of quadcopters have been investigated. Subsequently, using experiments in wind tunnel, a normalized model for the quadcopter drones was obtained which is independent from the disk load and the blade disks diameters. Then, for trajectory designs, a simple model is provided. Due to the complex optimal problem for minimum time trajectory design,

we designed optimal 2D and 3D trajectories for descent, using GPOPS-II package as a numerical solver. Finally, we performed flight experiments which showed that the VRS is present for quadcopters. In fact, this might be the cause of instability and crashes in fast descents. Furthermore, it is explained that by increasing the horizontal speed to the blade disk, the fluctuations can be reduced in the flight. By descending with a helix type trajectory as an optimal descending trajectory, the quadcopter can descend fast without entering to the unstable regions.

Possible directions for future work are to use learning methods to identify the unstable boundaries, controlling the quadcopter with learning methods, and investigating the behavior of variable pitch quadcopters in the VRS and WBS regions.

REFERENCES

- [1] G. Cai, J. Dias, and L. Seneviratne, "A survey of small-scale unmanned aerial vehicles: Recent advances and future development trends," *Unmanned Systems*, vol. 2, no. 02, pp. 175–199, 2014.
- [2] G. H. Saunders, *Dynamics of helicopter flight*. John Wiley & Sons, 1975.
- [3] W. Johnson, "Model for vortex ring state influence on rotorcraft flight dynamics," *NASA Ames Research Center*, 2005.
- [4] D. A. Peters and S.-Y. Chen, "Momentum theory, dynamic inflow, and the vortex-ring state," *Journal of the American Helicopter Society*, vol. 27, no. 3, pp. 18–24, 1982.
- [5] P.-M. Basset, C. Chen, J. Prasad, and S. Kolb, "Prediction of vortex ring state boundary of a helicopter in descending flight by simulation," *Journal of the American Helicopter Society*, vol. 53, no. 2, pp. 139–151, 2008.
- [6] G. J. Leishman, *Principles of helicopter aerodynamics with CD extra*. Cambridge university press, 2006.
- [7] J. Seddon and S. Newman, *Basic helicopter aerodynamics*. American Institute of Aeronautics and Astronautics, 2001.
- [8] H. Huang, G. M. Hoffmann, S. L. Waslander, and C. J. Tomlin, "Aerodynamics and control of autonomous quadrotor helicopters in aggressive maneuvering," in *Proceedings of IEEE International Conference on Robotics and Automation*, 2009, pp. 3277–3282.
- [9] O. Westbrook-Netherton and C. Toomer, "An investigation into predicting vortex ring state in rotary aircraft," *Royal Aeronautical Society*, 2014.
- [10] J. V. Foster and D. Hartman, "High-fidelity multi-rotor unmanned aircraft system (uas) simulation development for trajectory prediction under off-nominal flight dynamics," in *Proceedings of 17th AIAA Aviation Technology, Integration, and Operations Conference*, 2017, p. 3271.
- [11] G. M. Hoffmann, H. Huang, S. L. Waslander, and C. J. Tomlin, "Precision flight control for a multi-vehicle quadrotor helicopter testbed," *Control engineering practice*, vol. 19, no. 9, pp. 1023–1036, 2011.
- [12] L. Chenglong, F. Zhou, W. Jiafang, and Z. Xiang, "A vortex-ring-state-avoiding descending control strategy for multi-rotor uavs," in *Proceedings of 34th Chinese Control Conference (CCC)*, 2015, pp. 4465–4471.
- [13] J. Jimenez, A. Desopper, A. Taghizad, and L. Binet, "Induced velocity model in steep descent and vortex-ring state prediction," *Laboratoire ONERA-cole de L'Air*, 2001.
- [14] J. Prasad and C. Chen, "Prediction of vortex ring state using ring vortex model for single-rotor and multi-rotor configurations," in *Proceedings of AIAA Atmospheric Flight Mechanics Conference and Exhibit*, 2006, p. 6632.
- [15] S. Taamallah, "A qualitative introduction to the vortex-ring-state, autorotation, and optimal autorotation," in *Proceeding of 36th European Rotorcraft Forum, Paris, France*, 2010.
- [16] M. Bangura and R. Mahony, "Nonlinear dynamic modeling for high performance control of a quadrotor," in *Proceedings of Australasian Conference on Robotics and Automation, Victoria University of Wellington, New Zealand*. Australian Robotics and Automation Association, 2012.
- [17] M. Abildgaard and L. Binet, "Active sidesticks used for vortex ring state avoidance," in *Proceedings of 35th European Rotorcraft Forum*, 2009.
- [18] M. Ribera, "Helicopter flight dynamics simulation with a time-accurate free-vortex wake model," Ph.D. dissertation, 2007.
- [19] M. Hehn, R. Ritz, and R. D'Andrea, "Performance benchmarking of quadrotor systems using time-optimal control," *Autonomous Robots*, vol. 33, no. 1-2, pp. 69–88, 2012.
- [20] X. Liang, Y. Fang, N. Sun, and H. Lin, "Dynamics analysis and time-optimal motion planning for unmanned quadrotor transportation systems," *Mechatronics*, vol. 50, pp. 16–29, 2018.
- [21] S. K. Phang, S. Lai, F. Wang, M. Lan, and B. M. Chen, "Systems design and implementation with jerk-optimized trajectory generation for uav calligraphy," *Mechatronics*, vol. 30, pp. 65–75, 2015.
- [22] M. A. Patterson and A. V. Rao, "GPOPS-II: A MATLAB software for solving multiple-phase optimal control problems using hp-adaptive Gaussian quadrature collocation methods and sparse nonlinear programming," *ACM Transactions on Mathematical Software (TOMS)*, vol. 41, no. 1, p. 1, 2014.
- [23] W. Castles Jr and R. B. Gray, "Empirical relation between induced velocity, thrust, and rate of descent of a helicopter rotor as determined by wind-tunnel tests on four model rotors," *NACA TN 2474*, 1951.
- [24] P. F. Yaggy and K. W. Mort, *Wind-tunnel tests of two vtol propellers in descent*. National Aeronautics and Space Administration, 1963.
- [25] A. Azuma, J. Koo, T. Oka, and K. Washizu, "Experiments on a model helicopter rotor operating in the vortex ringstate," *Journal of Aircraft*, vol. 3, no. 3, pp. 225–230, 1966.
- [26] A. Taghizad, "Experimental and theoretical investigations to develop a model of rotor aerodynamics adapted to steep descents," in *Proceedings of American Helicopter Society 58th Annual Forum*, 2002.
- [27] A. Talaeizadeh, Y. Goodarzi, H. N. Pishkenari, and A. Alasty, "Accurate simulator for motion of the quadcopter; assuming dynamic and aerodynamic effects," in *Proceedings of the 27th Annual International Conference on Mechanical Engineering*, 2019, pp. 391–396.
- [28] H. Baruh, *Analytical dynamics*. WCB/McGraw-Hill Boston, 1999.
- [29] S. P. Sethi, *Optimal Control Theory*. Springer, 2019.



Amin Talaeizadeh received his B.Sc. and M.Sc. degrees in mechanical engineering from the Amir-kabir University of Technology, Tehran, Iran, in 2011 and 2013, respectively. He is currently pursuing the Ph.D. degree from the Sharif University of Technology, Tehran, Iran. He is now a visiting Ph.D. student in the CST group of Eindhoven University of Technology (TU/e). His current research interests include optimal trajectory design, robotics, model-based design, and optimal control.



Duarte Antunes received the Licenciatura in Electrical and Computer Engineering in 2005 and his Ph.D. in 2011 from the Instituto Superior Tecnico (IST), Lisbon, Portugal, in 2005. From 2011 to 2013 he held a postdoctoral position at the department of mechanical engineering at the Eindhoven University of Technology (TU/e), where he is currently an Assistant Professor.



Hossein Nejat Pishkenari earned his B.Sc., M.Sc. and Ph.D. degrees in Mechanical Engineering from the Sharif University of Technology in 2003, 2005 and 2010, respectively. Then he joined the Department of Mechanical Engineering at the Sharif University of Technology in 2012. Currently, he is directing the Nano-robotics Laboratory and the corresponding ongoing research projects in the multidisciplinary field of Nanotechnology.



Aria Alasty received his B.Sc. and M.Sc. degrees in Mechanical engineering from Sharif University of Technology (SUT), Tehran, Iran in 1987 and 1989. He also received his Ph.D. degree in Mechanical engineering from Carleton University, Ottawa, Canada, in 1996. At present, he is a professor of mechanical engineering in Sharif University of Technology. He has been a member of Center of Excellence in Design, Robotics, and Automation (CEDRA) since 2001. His fields of research are mainly in Non-linear and Chaotic systems control, Computational

Nano/Micro mechanics and control, special purpose robotics, robotic swarm control, and fuzzy system control.